American Journal of Applied Mathematics and Statistics, 2016, Vol. 4, No. 4, 99-107
Available online at http://pubs.sciepub.com/ajams/4/4/1

DOI:10.12691/ajams-4-4-1

Statistical Model of Polydisperse Fuel Spray in Three Dimensional Space

Ophir Nave*

Department of Mathematics, Ben-Gurion University of the Negev (BGU), PO Box 653 Beer-Sheva, 84105, Israel
*Corresponding author: naveof@cs.bgu.ac.il

Abstract In this study, we investigate the problem of the effects of droplets dispersion dynamics on ignition of polydisperse spray in turbulent mixing layers using probability density function. Studies of this problem have been found to be instrumental in developing understanding of turbulent combustion including the ignition of turbulent gaseous diffusion flames. The parameters used to describe the distribution of droplet sizes are the moments of the droplet size distribution function which are allowed to vary in the fourth vector (x, y, z, t). In our analysis we applied the Homotopy Analysis Method. This method contains a certain auxiliary parameter $\hbar$ which provides a way to control the convergence region and the rate of convergence of the series solutions.

Keywords: *partial differential equations, polydisperse fuel spray, laminar boundary layer, Homotopy Analysis Method*

Cite This Article: Ophir Nave, "Statistical Model of Polydisperse Fuel Spray in Three Dimensional Space." *American Journal of Applied Mathematics and Statistics*, vol. 4, no. 4 (2016): 99-107. doi: 10.12691/ajams-4-4-1.

1. Introduction

When modeling the polydisperse spray one can employ the discrete droplet model. One method is to solve the governing equations of motion for turbulent carrier gas in an Eulerian scheme, and then to integrate Lagrangian equations of motion for liquid droplets along true path lines [1,2,3,4]. The advantages of this method are the ability to efficiently discretize the liquid phase (i.e., spray) into groups of identical droplets, each containing droplets of a given radius, and the fact that the equations for the dispersed liquid phase are more naturally written down in a Lagrangian manner. Another method is the well known Eulerian-Eulerian scheme. This method has been used by many researchers such as [5,6,7]. This approach is useful in the case when the flow contains many collisions between the droplets. In addition, when applying this method, one should assume a local equilibrium between the two phases. Another useful method is the stochastic approach. The spray is described by the distribution function (or density function) $f_j(r,\vec{x},\vec{v},t)drd\vec{x}d\vec{v}$, which is the probable number of particles of chemical composition j in the radius range dr about r located in the spatial range $d\vec{x}$ about $\vec{x}$ with velocities in the range $d\vec{v}$ about $\vec{v}$ at time t, [8].

When formulating the model, the source terms include and describe effects of droplets breakup and the effects on the gas phase. In order to evaluate the velocity, the rate change of velocity, the radius, and the energy, one should write the governing equations in the Lagrangian forms. An Eulerian conservation equation is then written for the number density f_j in each considered range j, integrating over the radius range and taking a delta-function approach [9].

In this paper we modeled the polydisperse spray using the moments of the droplet-size-number distribution. The advantages of this approach are as follows: 1. the number of equations that must be solved is significantly less compared to other methods reviewed above, 2. using the moments means that the polydisperse spray is dealt with in terms of average quantities which allows a smooth representation of the droplet-size at all points, rather than a discrete representation [10,11,12,13].

2. Physical Assumptions and Conservation Equations

The physical model describes the thermal ignition of polydisperse fuel spray in a two-dimensional laminar mixing layer. The parameters used to describe the distribution of droplet sizes are the moments of the droplet size distribution function which are allowed to vary in space and time. Droplet breakup, and droplet droplet collisions effects are ignored. The vaporization time $t_v = \left(\frac{\rho_l}{\rho_A}\right)\frac{R_0^2}{3D_{TA}}$ is used to define the length scales for the longitudinal and transverse coordinates x and y. A Fickian description is used for the diffusion velocities of all species, with the binary diffusivity of species i into the mixture D_i' scaled with its air side value to give $D_i' = D_i' / D_{iA}$. We assumed the power -law dependence $\rho D_i = T^{\sigma}$ for the transport properties. The equation of state can be written in terms of the mass fraction of the fuel Y_F in the form of

$\rho T\left(1-Y_F\left(1-W_A/W_F\right)\right)=1$. For simplicity, the chemistry describing the thermal ignition process is an irreversible reaction between the Oxygen of the air and the fuel vapor in the form of $F+sO_2\rightarrow(1+s)P+Q$ where s and Q are the mass of Oxygen consumed and the amount of heat released per unit mass of fuel burned respectively. Under the above assumptions, the gas phase dimensionless conservation equations are:

$$\nabla_{\vec{x}^*}\cdot\left(\rho^*\vec{w}^*\right)=\alpha\Lambda\left\langle r^*\right\rangle\circ 1, \tag{2.1}$$

$$\nabla_{\vec{x}^*}\cdot\left(\rho^*u^*\vec{w}^*\right)=Pr\frac{\partial}{\partial y^*}\left(T^{*\sigma}\frac{\partial u^*}{\partial y^*}\right)+\alpha\Lambda\left\langle r^*u_d^*\right\rangle\circ 1 -\frac{3\alpha}{2}PrT^{*\sigma}\left\langle r^*\right\rangle[u^*-u_d^*], \tag{2.2}$$

$$\nabla_{\vec{x}^*}\cdot\left(\rho^*Y_F^*\vec{w}^*\right)=\frac{1}{Le_F}\frac{\partial}{\partial y^*}\left(T^{*\sigma}\frac{\partial Y_F^*}{\partial y^*}\right) +\alpha\Lambda\left\langle r^*\right\rangle\circ 1-\rho^*{Y_o}^*Y_F^*e^{\beta\frac{(T^*-1)}{T^*}}, \tag{2.3}$$

$$\nabla_{\vec{x}^*}\cdot\left(\rho^*{Y_o}^*\vec{w}^*\right)=\frac{\partial}{\partial y^*}\left(T^{*\sigma}\frac{\partial {Y_o}^*}{\partial y^*}\right) -S^*\rho^*{Y_o}^*Y_F^*e^{\beta\frac{(T^*-1)}{T^*}}, \tag{2.4}$$

$$\nabla_{\vec{x}^*}\cdot\left(\rho^*T^*\vec{w}^*\right)=\frac{\partial}{\partial y^*}\left(T^{*\sigma}\frac{\partial T^*}{\partial y^*}\right)-\alpha\Lambda\left\langle r^*\right\rangle\circ\left[l_v^*-T_d^*\right] -\alpha T^{*\sigma}\left\langle r^*\right\rangle\circ\left[T^*-T_d^*\right] +q^*\rho^*{Y_o}^*Y_F^*e^{\beta\frac{(T^*-1)}{T^*}}, \tag{2.5}$$

and the conservation equations for the liquid phase are:

$$\nabla_{\vec{x}^*}\cdot\left(\left\langle r^{*3}\right\rangle\circ\vec{w}_d^*\right)=-\Lambda\left\langle r^*\right\rangle\circ 1, \tag{2.6}$$

$$\nabla_{\vec{x}^*}\cdot\left(\left\langle r^{*3}\right\rangle\circ u_d^*\vec{w}_d^*\right)=\frac{3}{2}PrT^{*\sigma}\left\langle r^*\right\rangle\circ\left[u^*-u_d^*\right] -\Lambda\left\langle r^*\right\rangle\circ u_d^*, \tag{2.7}$$

$$\nabla_{\vec{x}^*}\cdot\left(\left\langle r^{*3}\right\rangle\circ v_d^*\vec{w}_d^*\right)=\frac{3}{2}PrT^{*\sigma}\left\langle r^*\right\rangle\circ\left[v^*-v_d^*\right] -\Lambda\left\langle r^*\right\rangle\circ v_d^*, \tag{2.8}$$

$$\nabla_{\vec{x}^*}\cdot\left(\left\langle r^{*3}\right\rangle\circ T_d^*\vec{w}_d^*\right)=\frac{c_p}{c_l}T^{*\sigma}\left\langle r^*\right\rangle\circ\left[T^*-T_d^*\right] -\Lambda\left\langle r^*\right\rangle\circ T_d^*, \tag{2.9}$$

where $\Lambda=T^{*\sigma}ln\left[1+\frac{(T-T_B)}{l_v}\right]$.

The initial conditions at $x=0$ and $y>0$ are:

$$u^*-1=Y_F^*={Y_o}^*-1=T^*-1=0, \tag{2.10}$$

and

$$u^*-u_s^*=Y_F^*=T^*-T_B^*=T_d^*-T_B^* =u_d^*=u_s^*=v_d^*={Y_o}^*-{Y_{o_s}}^*=0, \tag{2.11}$$

for $y<0$, and the boundary condition for $x>0$ is given by

$$u^*-1=Y_F^*={Y_o}^*-1=T^*-1=0, \tag{2.12}$$

as $y\rightarrow\infty$, and

$$u^*-u_s^*=Y_F^*={Y_o}^*-{Y_{o_s}}^*=T^*-T_B^*=v^*=0, \tag{2.13}$$

for $y\rightarrow-\infty$.

The initial distribution is taken to be Gaussian.

The dimensionless variables are as follows:

$$r^*=\frac{R}{R_0},R_0=\left(\frac{\int_0^\infty R^3P_{R0}dR}{\int_0^\infty P_{R0}dR}\right)^{1/3},\tilde{P}=\frac{R_0}{n_{d0}}P_{R0}$$

$${Y_o}^*=Y_o/Y_{o_{2A}},\beta=\frac{E}{BT_A},S^*=\frac{s}{Y_{o_{2A}}},$$

$$l_v^*=\frac{L_v}{c_pT_A},q^*=\frac{Q}{c_pT_A},$$

$$y^*=\frac{y}{\sqrt{D_{T_A}t_v}},,x^*=\frac{x}{U_At_v}u^*=\frac{u}{U_A},u_d^*=\frac{u_d}{U_A} \tag{2.14}$$

$$v^*=\frac{v}{\sqrt{\frac{D_{T_A}}{t_v}}},v_d^*=\frac{v_d}{\sqrt{\frac{D_{T_A}}{t_v}}},T^*=\frac{T}{T_A},T_d^*=\frac{T_d}{T_A},\rho^*=\frac{\rho}{\rho_A}$$

$$t_v^*=\left(\frac{\rho_l}{\rho_A}\right)\frac{R_0^2}{3D_{T_A}}.$$

The following notations are used for the above model: B universal gas constant, c specific heat capacity, D thermal diffusivity, E activation energy, L_v latent heat of vaporization, Le Lewis number, n dimensionless droplet-number density, P probability density function, Pr Prandtl number, Q heat of combustion, R droplet radius, r dimensionless droplet radius, S mass of air consumed per unit mass of fuel burned, T gas temperature, u gas velocity (longitudinal component), U mean stream velocity, v gas velocity (transverse component), $\vec{w}$ =(u, v), x longitudinal coordinate, y transverse coordinate, Y mass fraction, W molecular mass, $\vec{x}$ =(x, y), $\left\langle f(R)\right\rangle\circ g(\cdot)=\int_0^\infty f(R)P(\vec{x},R)g(\cdot)dR$ or $\int_0^\infty\tilde{f}(r)\tilde{P}(\vec{x},r)\tilde{g}(\cdot)dr$ in dimensionless terms, ∇ two dimensional gradient, ρ density, α the ratio of mass of liquid per unit volume to the gas density $\alpha=\frac{4}{3}\pi R_0^3n_{d0}\rho_l/\rho_A$ (dimensionless), σ relate to a power law. Subscripts: 0 initial, A air, B boiling, d

droplet, l liquid, F Fuel, o oxygen, p under constant pressure, s spray.

3. Homotopy Analysis Method-HAM

1. *Preliminaries*

The application of the HAM to a system of non linear partial differential equations is as follows [15,16]: Let

$$N_i[u_1(\vec{r}),u_2(\vec{r}),...,u_n(\vec{r})],i=1,...,n, \tag{3.1}$$

be a system of differential equations with the initial conditions:

$$u_i(\vec{0})=u_{i0},i=1,...,n, \tag{3.2}$$

where N_i are nonlinear operators, $\vec{r}$ independent variables and u_i are unknown functions. The zero-order deformation equations for $i=1,...,n$ are:

$$\begin{aligned}&(1-p)L_i[\varphi_i(\vec{r};p)-u_{i0}(\vec{r})]\\&-p\hbar_i H_i(\vec{r})N_i[\varphi_1(\vec{r}),\varphi_2(\vec{r}),...,\varphi_n(\vec{r})]=0,\end{aligned} \tag{3.3}$$

where $p\in[0,1]$ is the embedding parameter, $\hbar_i$ are the non zero auxiliary parameters, $H_i\neq 0$ are non zero auxiliary functions, L_i are the auxiliary linear operators and $u_{i0}(\vec{r})$ are the initial conditions of $u_i(\vec{r})$. According to (3.3), when $p=0$ and $p=1$, it holds $\varphi_i(\vec{r};0)=u_{i0}(\vec{r})$ and $\varphi_i(\vec{r};1)=u_i(\vec{r})$ $i=1,...,n$. Which means that when p varies from 0 to 1, the solution $\varphi_i(\vec{r};p)$ varies from the initial condition $u_{i0}(\vec{r})$ to the solution $u_i(\vec{r})$. Expanding $\varphi_i(\vec{r};p)$ to a power series with respect to the small parameter p,

$$\varphi_i(\vec{r};p)=u_{i0}(\vec{r})+\sum_{m=0}^{\infty}u_{im}(\vec{r})p^m,i=1,...,n, \tag{3.4}$$

where

$$\begin{aligned}u_{im}(\vec{r})&=\frac{1}{m!}\frac{\partial^m\varphi_i(\vec{r};p)}{\partial p^m}|_{p=0}\\&\equiv D_m(\varphi_i(\vec{r};p))|_{p=0},i=1,...,n.\end{aligned} \tag{3.5}$$

When $p=1$ the series in (3.5) convergence to the solution and we have:

$$u_{im}(\vec{r})=u_{i0}(\vec{r})+\sum_{m=0}^{\infty}u_{im}(\vec{r}),i=1,...,n,i=1,...,n. \tag{3.6}$$

In order to obtain a series solution of HAM, define the vector:

$$\vec{u}_{im}(\vec{r})=\{u_{i0}(\vec{r}),u_{i1}(\vec{r}),...,u_{in}(\vec{r})\},i=1,...,n. \tag{3.7}$$

Differentiating Equation (3.3) m-times with respect to the embedding parameter p, setting $p=0$ and finally dividing the terms by $m!$, we obtain the m th-order deformation equations in the form of:

$$\begin{aligned}&L_i[u_{im}(\vec{r})-\chi_m u_{im-1}(\vec{r})]\\&-\hbar_i H_i(\vec{r})R_{im}(\vec{u}_{1m-1},...,\vec{u}_{nm-1},\vec{r})=0,\end{aligned} \tag{3.8}$$

where,

$$\begin{aligned}&R_{im}(\vec{u}_{1m-1},\vec{u}_{2m-1},...,\vec{u}_{nm-1},\vec{r})\\&=\frac{1}{(m-1)!}\frac{\partial^{m-1}N_i(\varphi_1(\vec{r};p),...,\varphi_n(\vec{r};p))}{\partial p^{m-1}}|_{p=0},\end{aligned} \tag{3.9}$$

and χ_m is the unit step function. Applying the inverse operator $L_i^{-1}(\cdot)$ on both sides of Equation (3.8), we obtain

$$\begin{aligned}&u_{im}(\vec{r})=\chi_m u_{im-1}(\vec{r})\\&+\hbar_i L_i^{-1}[H_i(\vec{r})R_{im}(\vec{u}_{1m-1},...,\vec{u}_{nm-1},\vec{r})].\end{aligned} \tag{3.10}$$

The solution of the m th-order deformation can be expressed according to Equation (3.10) which can be solved by symbolic software such as Mathematica 8.0, Maple, Matlab and so on. When one substitutes the $u_{im}(\vec{r})$ for $m\geq 1$, then the M -order series is

$$u_i(\vec{r})=\sum_{m=0}^{M}u_{im}(\vec{r}), \tag{3.11}$$

and when $M\to\infty$, then one can obtain an accurate approximation of the original system (3.1).

2. *Application*

In order to apply the HAM to the model (2.1)-(2.9) (for convenience we ignore the asterisk from the model) let us define the following series:

$$\begin{aligned}\varphi_1(x,y;p)&=\sum_{m=0}^{\infty}u_m(x,y)p^m,\varphi_2(x,y;p)\\&=\sum_{m=0}^{\infty}v_m(x,y)p^m,\\\varphi_3(x,y;p)&=\sum_{m=0}^{\infty}T_m(x,y)p^m,\varphi_4(x,y;p)\\&=\sum_{m=0}^{\infty}u_{dm}(x,y)p^m,\\\varphi_5(x,y;p)&=\sum_{m=0}^{\infty}v_{dm}(x,y)p^m,\varphi_6(x,y;p)\\&=\sum_{m=0}^{\infty}r_m(x,y)p^m,\\\varphi_7(x,y;p)&=\sum_{m=0}^{\infty}Y_{Fm}(x,y)p^m,\varphi_8(x,y;p)\\&=\sum_{m=0}^{\infty}Y_{om}(x,y)p^m.\\\varphi_9(x,y;p)&=\sum_{m=0}^{\infty}T_{dm}(x,y)p^m.\end{aligned} \tag{3.12}$$

We choose the linear operators L_i as

$$L_i[\varphi_i]=\nabla_{\vec{x}}\varphi_i,i=1,...,9, \tag{3.13}$$

with the property $L_i(c_i)=0$ $(i=1,...,9)$, where c_i $(i=1,...,9)$ are integral constants. The non linear operators N_i $(i=1,...,9)$ of the considered system are defined as:

$$N_1[\varphi_1,...,\varphi_9]=\nabla_{\vec{x}}\cdot\left(\rho(\varphi_1,\varphi_2)\right)-\alpha\Lambda\langle\varphi_6\rangle\circ 1, \tag{3.14}$$

$$N_2[\varphi_1,...,\varphi_9]=\nabla_{\vec{x}}\cdot\left(\rho\varphi_1(\varphi_1,\varphi_2)\right)-Pr\frac{\partial}{\partial y}\left(\varphi_3^{\sigma}\frac{\partial\varphi_1}{\partial y}\right) \quad (3.15)$$
$$-\alpha\Lambda\left\langle\varphi_6\varphi_4\right\rangle\circ 1+\frac{3\alpha}{2}Pr\varphi_3^{\sigma}\left\langle\varphi_6\right\rangle[\varphi_1-\varphi_4],$$

$$N_3[\varphi_1,...,\varphi_9]=\nabla_{\vec{x}}\cdot\left(\varphi_7(\varphi_1,\varphi_2)\right)-\frac{1}{Le_F}\frac{\partial}{\partial y}\left(\varphi_3^{\sigma}\frac{\partial\varphi_7}{\partial y}\right) \quad (3.16)$$
$$-\alpha\Lambda\left\langle\varphi_6\right\rangle\circ 1+\rho\varphi_8\varphi_7 e^{\beta\frac{(\varphi_3-1)}{\varphi_3}},$$

$$N_4[\varphi_1,...,\varphi_9]=\nabla_{\vec{x}}\cdot\left(\rho\varphi_8(\varphi_1,\varphi_2)\right)-\frac{\partial}{\partial y}\left(\varphi_3^{\sigma}\frac{\partial\varphi_8}{\partial y}\right) \quad (3.17)$$
$$+\rho\varphi_8\varphi_7 e^{\beta\frac{(\varphi_3-1)}{\varphi_3}},$$

$$N_5[\varphi_1,...,\varphi_9]=\nabla_{\vec{x}}\cdot\left(\rho\varphi_3(\varphi_1,\varphi_2)\right)-\frac{\partial}{\partial y}\left(\varphi_3^{\sigma}\frac{\partial\varphi_3}{\partial y}\right)$$
$$+\alpha\Lambda\left\langle\varphi_6\right\rangle\circ\left[l_v-\varphi_9\right]\alpha\varphi_3^{\sigma}\left\langle\varphi_6\right\rangle\circ\left[\varphi_3-\varphi_9\right] \quad (3.18)$$
$$-q\rho\varphi_8\varphi_7 e^{\beta\frac{(\varphi_3-1)}{\varphi_3}},$$

$$N_6[\varphi_1,...,\varphi_9]=\nabla_{\vec{x}}\cdot\left(\left\langle\varphi_3^3\right\rangle\circ(\varphi_4,\varphi_5)\right)+\Lambda\left\langle\varphi_3\right\rangle\circ 1, \quad (3.19)$$

$$N_7[\varphi_1,...,\varphi_9]=\nabla_{\vec{x}}\cdot\left(\left\langle\varphi_6^3\right\rangle\circ\varphi_4(\varphi_4,\varphi_5)\right)$$
$$-\frac{3}{2}Pr\varphi_3^{\sigma}\left\langle\varphi_6\right\rangle\circ\left[\varphi_1-\varphi_4\right] \quad (3.20)$$
$$+\Lambda\left\langle\varphi_6\right\rangle\circ\varphi_4,$$

$$N_8[\varphi_1,...,\varphi_9]=\nabla_{\vec{x}}\cdot\left(\left\langle\varphi_6^3\right\rangle\circ\varphi_5(\varphi_4,\varphi_5)\right)$$
$$-\frac{3}{2}Pr\varphi_3^{\sigma}\left\langle\varphi_6\right\rangle\circ\left[\varphi_2-\varphi_5\right] \quad (3.21)$$
$$+\Lambda\left\langle\varphi_6\right\rangle\circ\varphi_5,$$

$$N_9[\varphi_1,...,\varphi_9]=\nabla_{\vec{x}}\cdot\left(\left\langle\varphi_6^3\right\rangle\circ\varphi_9(\varphi_4,\varphi_5)\right)$$
$$-\frac{c_p}{c_l}\varphi_3^{\sigma}\left\langle\varphi_6\right\rangle\circ\left[\varphi_3-\varphi_9\right] \quad (3.22)$$
$$+\Lambda\left\langle\varphi_6\right\rangle\circ\varphi_9.$$

Using the above non linear operators, and using the assumption that $H_i=1$ $(i=1,...,9)$, we construct the m-order deformation equations in the form of:

$$L_i[\psi_{im}(\vec{r})]-\chi_m\psi_{im-1}(\vec{x})]-\hbar_i R_{im}(\vec{\Psi}_{m-1})=0, \quad (3.23)$$

where $\psi_{im}(\vec{r})$ $(i=1,...,9)$ present the functions:

$$u_m(\vec{x}),v_m(\vec{x}),T_m(\vec{x}),u_{dm}(\vec{x}),v_{dm}(\vec{x}),$$
$$r_m(\vec{x}),Y_{Fm}(\vec{x}),Y_{om}(\vec{x}),T_{dm}(\vec{x}), \quad (3.24)$$

and $\vec{\Psi}_{m-1}$ presents the functions:

$$\vec{u}_{m-1},\vec{v}_{m-1},\vec{T}_{m-1},\vec{u}_{dm-1},\vec{v}_{dm-1},$$
$$\vec{r}_{m-1},\vec{Y}_{Fm-1},\vec{Y}_{om-1},\vec{T}_{dm-1}. \quad (3.25)$$

The expressions R_{im} in Equation (3.23) are as follows:

$$R_{1m}=\nabla_{\vec{x}}\cdot(\rho(u_{m-1},v_{m-1}))-\alpha\Lambda\left\langle r_{m-1}\right\rangle\circ 1, \quad (3.26)$$

$$R_{2m}=\nabla_{\vec{x}}\cdot(\rho(\sum_{i=0}^{m}u_iu_{m-i},\sum_{i=0}^{m}u_iv_{m-i}))$$
$$-Pr\frac{\partial}{\partial y}\left(\sum_{i=0}^{m}T_i\frac{\partial u_{m-i}}{\partial y}\right) \quad (3.27)$$
$$+\frac{3\alpha}{2}Pr\sum_{i=0}^{m}T_i\left(\sum_{k=0}^{m-i}\left\langle r_k\right\rangle\circ\left[u_{m-i-k}-u_{dm-i-k}\right]\right),$$

$$R_{3m}=\nabla_{\vec{x}}\cdot(\rho(\sum_{i=0}^{m}Y_{Fi}u_{m-i},\sum_{i=0}^{m}Y_{Fi}v_{m-i}))$$
$$-\frac{1}{Le_F}\frac{\partial}{\partial y}\left(\sum_{i=0}^{m}T_i\frac{\partial Y_{Fm-i}}{\partial y}\right)-\alpha\Lambda\left\langle r_{m-1}\right\rangle\circ 1 \quad (3.28)$$
$$+\rho\sum_{i=0}^{m}Y_{oi}\sum_{k=0}^{m-i}Y_{Fk}\sum_{j=0}^{m-i-k-1}\left[\begin{array}{l}\left(1-\frac{j}{m-i-k}\right)\\ D_j\left(e^T\right)D_{m-i-k-j}(T)\end{array}\right],$$

$$R_{4m}=\nabla_{\vec{x}}\cdot(\rho(\sum_{i=0}^{m}Y_{oi}u_{m-i},\sum_{i=0}^{m}Y_{oi}v_{m-i}))$$
$$-\frac{1}{Le_F}\frac{\partial}{\partial y}\left(\sum_{i=0}^{m}T_i\frac{\partial Y_{om-i}}{\partial y}\right) \quad (3.29)$$
$$+S\rho\sum_{i=0}^{m}Y_{oi}\sum_{k=0}^{m-i}Y_{Fk}\sum_{j=0}^{m-i-k-1}\left[\begin{array}{l}\left(1-\frac{j}{m-i-k}\right)\\ D_j\left(e^T\right)D_{m-i-k-j}(T)\end{array}\right],$$

$$R_{5m}=\nabla_{\vec{x}}\cdot(\rho(\sum_{i=0}^{m}T_iu_{m-i},\sum_{i=0}^{m}T_iv_{m-i}))$$
$$-\frac{\partial}{\partial y}\left(\sum_{i=0}^{m}T_i\frac{\partial T_{m-i}}{\partial y}\right)+\alpha\Lambda\left(\left\langle r_{m-1}\right\rangle_v-\sum_{i=0}^{m}\left\langle r_i\right\rangle\circ T_{dm-i}\right)$$
$$+\alpha\sum_{i=0}^{m}T_i\sum_{k=0}^{m-i}\sum_{k=0}^{m-i}\left\langle r_k\right\rangle\circ[T_{m-i-k}-T_{dm-i-k}], \quad (3.30)$$
$$-q\rho\sum_{i=0}^{m}Y_{oi}\sum_{k=0}^{m-i}Y_{Fk}\sum_{j=0}^{m-i-k-1}\left[\begin{array}{l}\left(1-\frac{j}{m-i-k}\right)\\ D_j\left(e^T\right)D_{m-i-k-j}(T)\end{array}\right],$$

$$R_{6m}=\nabla_{\vec{x}}\cdot(\sum_{i=0}^{m}\left\langle r_i^3\right\rangle\circ u_{dm-1},\sum_{i=0}^{m}\left\langle r_i^3\right\rangle\circ v_{dm-1})) \quad (3.31)$$
$$+\alpha\Lambda\left\langle r_{m-1}\right\rangle\circ 1,$$

$$R_{7m}=\nabla_{\vec{x}}\cdot\left(\begin{array}{l}\sum_{i=0}^{m}\left\langle r_i^3\right\rangle\circ\sum_{k=0}^{m-i}u_{dk}u_{dm-i-k},\\ \sum_{i=0}^{m}\left\langle r_i^3\right\rangle\circ\sum_{k=0}^{m-i}u_{dk}v_{dm-i-k}\end{array}\right)$$
$$-\frac{3}{2}Pr\sum_{i=0}^{m}T_i\left(\sum_{k=0}^{m-i}\left\langle r_k\right\rangle\circ[u_{m-i-k}-u_{dm-i-k}]\right) \quad (3.32)$$
$$+\Lambda\sum_{i=0}^{m}\left\langle r_i\right\rangle\circ u_{dm-i},$$

$$R_{8m} = \nabla_{\vec{x}} \cdot \begin{pmatrix} \sum_{i=0}^{m} \left\langle r_i^3 \right\rangle \circ \sum_{k=0}^{m-i} v_{dk} u_{dm-i-k}, \\ \sum_{i=0}^{m} \left\langle r_i^3 \right\rangle \circ \sum_{k=0}^{m-i} v_{dk} v_{dm-i-k} \end{pmatrix}$$
$$-\frac{3}{2} Pr \sum_{i=0}^{m} T_i \left(\sum_{k=0}^{m-i} \left\langle r_k \right\rangle \circ [v_{m-i-k} - v_{dm-i-k}] \right) \quad (3.33)$$
$$+\Lambda \sum_{i=0}^{m} \left\langle r_i \right\rangle \circ v_{dm-i},$$

$$R_{9m} = \nabla_{\vec{x}} \cdot \begin{pmatrix} \sum_{i=0}^{m} \left\langle r_i^3 \right\rangle \circ \sum_{k=0}^{m-i} T_{dk} u_{dm-i-k}, \\ \sum_{i=0}^{m} \left\langle r_i^3 \right\rangle \circ \sum_{k=0}^{m-i} T_{dk} v_{dm-i-k} \end{pmatrix}$$
$$-\frac{c_p}{c_l} \sum_{i=0}^{m} T_i \left(\sum_{k=0}^{m-i} \left\langle r_k \right\rangle \circ [T_{m-i-k} - T_{dm-i-k}] \right) \quad (3.34)$$
$$+\Lambda \sum_{i=0}^{m} \left\langle r_i \right\rangle \circ T_{dm-i}.$$

By using the software Matlab one can obtain the solutions using Equation (3.10) for each function in Equation (3.24) and finally one should substitute the appropriate expressions in Equations (3.11).

4. Analysis and Results

In our analysis we compared between two polydisperse fuel spray: Heptane and Methanol. The values of the dimensionless parameters are [14]: 1. *Heptane* : $q = 39.5$, $l_v = 0.34$, $T_B = 0.37$, $c = 2.2$, $W_A / W_F = 0.29$, $Le_F = 2.6$, $S = 15.2$, and 2. *Methanol* : $q = 18.6$, $l_v = 1.09$, $T_B = 0.34$, $c = 2.5$, $W_A / W_F = 0.91$, $Le_F = 1.2$, $S = 6.5$.

The air-side temperature is assumed to be $T_A = 1000K$. The rest of the parameters are: $\alpha = 1$, $Pr = 0.7$, $\beta = 10$ and $T_S = T_B$.

We have implemented the numerical method for PDE using the software MATLAB. Our results are presented in Figures (4.1)-(4.3) for different contour lines in the $x - y$ plane. In all cases, the polydisperse spray mixes with the hot air without any appreciable chemical reaction. The vaporization process of the different size droplets is caused by coflowing of hot air stream. The fuel vapor diffuses into the air stream, and then it starts to react with the oxygen as it reaches the high temperature boundary, which is far away from the polydisperse spray. In Figure (4.1) we plot the temperatures T and T_d . The air stream temperature is decreased at the beginning of the process (when the spray and the hot air are mixed) because the different initial values for both fuels (heptane and methanol) (Figures (4.1)-(a) and (4.1)-(b)). The methanol decreases more slowly. On the other hand, the droplets temperature T_d is increased because of the hot air (Figure (4.1)). The droplets temperature of theheptane is increase more faster in compare to increases at a faster rate, in comparison to the methanol (Figure (4.1)-(c) and Figure (4.1)-(d)) respectively. The three dimensional surfaces of the gas and droplets temperature are presented in Figure (4.4).

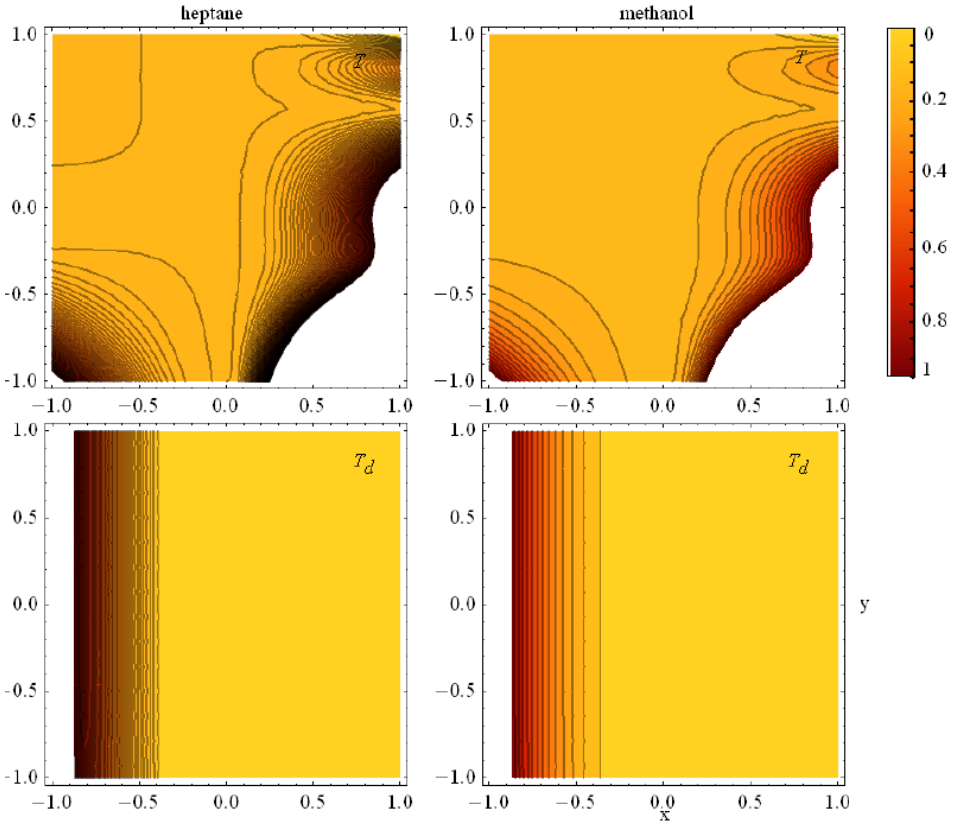

Figure (4.1). Solution profiles of the temperature for heptane and methanol

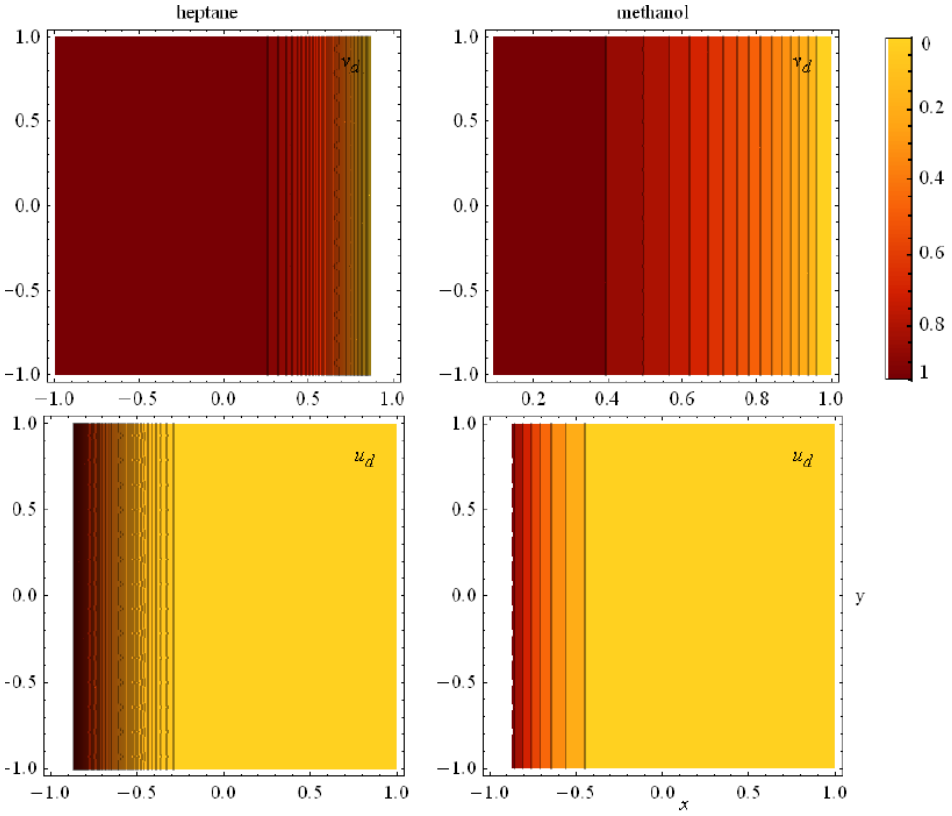

Figure (4.2). Solution profiles of the velocity in x and y directions for heptane and methanol

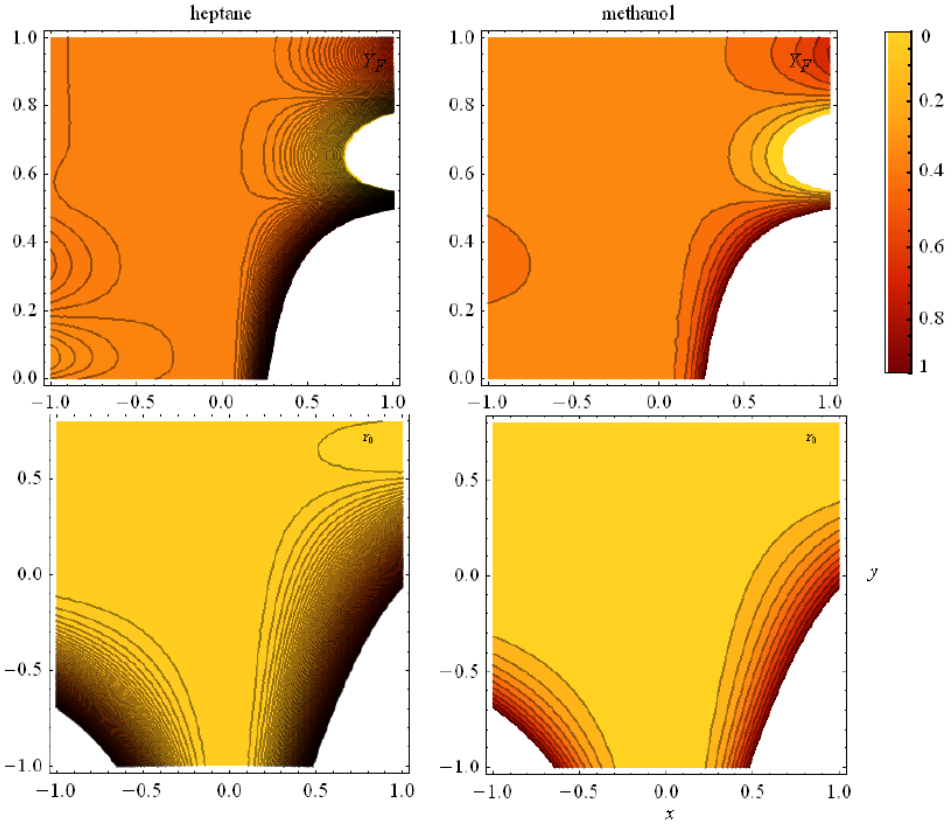

Figure (4.3). Solution profiles of the mass fraction of oxygen and fuel

The droplets velocity u_d and v_d in x and y directions respectively start from the initial conditions and then decrease because of the interaction of the droplets with the hot air (friction). The velocity in v_d of the methanol is the first to decrease (Figure (4.2)-(b)) as compared to the heptane (Figure (4.2)-(a)). The velocity u_d of both the heptane and methanol decreases at a slower rate, in comparison to the v_d. These results are compatible with the three dimensional surfaces presented in Figures (4.5). The droplet velocity v_d is decreases close to the initial conditions.

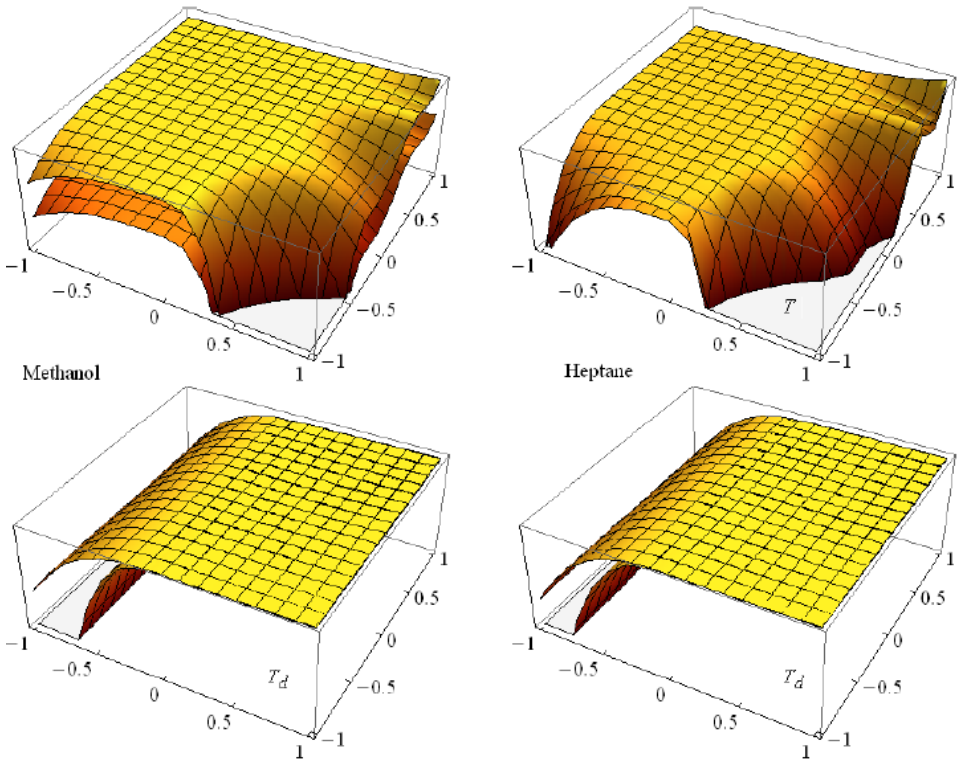

Figure (4.4). Solution profiles of the droplets and gas temperature in three-dimensional space. The upper surface is the solution of the model Equations (2.1)-(2.9) obtained by applying numerical simulations, and the lower surface is the solution of the model (2.1)-(2.9) obtained by applying the homotopy analysis method (HAM)

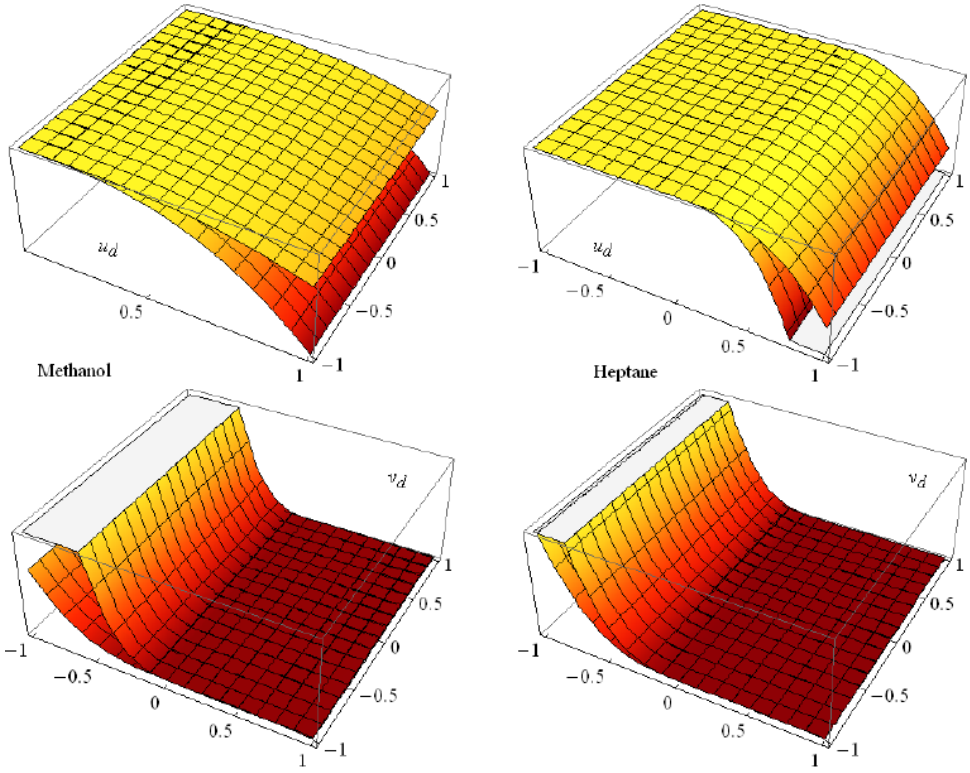

Figure (4.5). Solution profiles of the droplets velocity in three-dimensional space. The upper surface is the solution of the model Equations (2.1)-(2.9) obtained by applying numerical simulations, and the lower surface is the solution of the model (2.1)-(2.9) obtained by applying the homotopy analysis method (HAM)

The solution profiles of the mass fraction of oxygen and fuel and the differences between the heptane and methanol are shown in Figures (4.3). The coordinate x of the ignition is $x \in (0.4-0.6)$ and this result is compatible with the solution profiles of the temperature, velocity and mass fraction (Figures (4.1)-(4.3)).

In our analysis we assumed that the probability density function P_R does not change in time due to the scales selected [14] (short period of ignition).

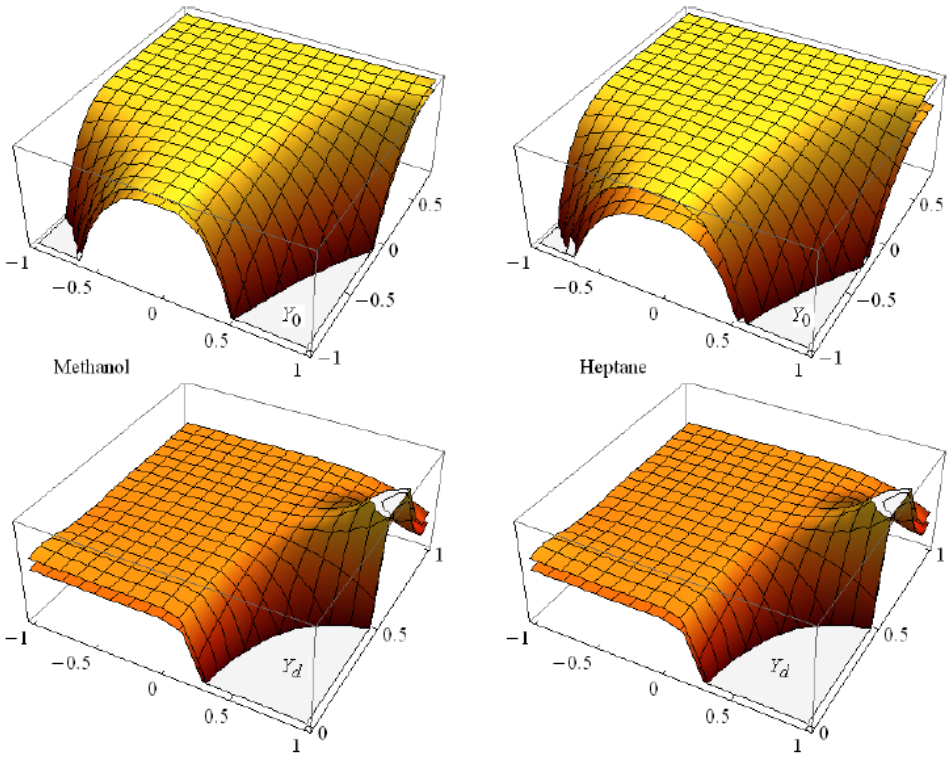

Figure (4.6). Solution profiles of the mass fraction of Oxygen and Fuel in three-dimensional space. The upper surface is the solution of the model Equations (2.1)-(2.9) obtained by applying numerical simulations, and the lower surface is the solution of the model (2.1)-(2.9) obtained by applying the homotopy analysis method (HAM)}

In our Analysis, in addition to numerical simulations, we applied the homotopy analysis method. In Figures (4.4)-(4.6) the upper surfaces are the solution of the model given in Equations (2.1)-(2.9) obtained by applying numerical simulations, and the lower surfaces are the solution of the model given in Equations (2.1)-(2.9) obtained by applying the homotopy analysis method (HAM). As can be seen by these figures, the solutions that are obtained by the HAM series are close to the numerical solutions. The great freedom and flexibility to choose the auxiliary convergence control parameter, the auxiliary linear operators and the non zero auxiliary functions increase the possibility of finding satisfactory series solutions which are very close to the numerical ones. To summarize, the homotopy analysis method (HAM) is an analytical approach for obtaining convergent series solutions of strongly nonlinear problems. It is also a method which economizes the computer processing work time. In general it is impossible to solve high-order deformation equations quickly while maintaining an approximation at a high enough order without a high-performance computer. Furthermore, it is also impossible to choose a proper value of the convergence- control parameter without the use of symbolic computers software.

5. Conclusions

In this study, we investigated the problem of the effects of droplets dispersion dynamics on ignition of polydisperse spray in turbulent mixing layers using probability density function. In our analysis we compared two polydisperse fuel sprays: Heptane and Methanol.

We applied an analytic technique, known as the homotopy analysis method (HAM). The major advantage of this method is that there is no need for the emergence of a small parameter in the model. The artificial parameter that this method utilizes provides a method for controlling the convergence region and rate of convergence of the series solutions.

There is a high degree of agreement between our theoretical results and the numerical results of the technique.

This present research shows the validity and the enormous potential of the homotopy analysis method for nonlinear problems in science and engineering.

Acknowledgements

This research was supported by the department of mathematics and physics at the Academic Lev Center and Ben Gurion University.

Nomenclature

B	universal gas constant
c	specific heat capacity
D	thermal diffusivity
E	activation energy
L_v	latent heat of vaporization
L_e	Lewis number
n	dimensionless droplet-number density
P	probability density function
P_r	Prandtl number
Q	heat of combustion
R	droplet radius
r	dimensionless droplet radius

S	mass of air consumed per unit mass of fuel burned
T	gas temperature
u	gas velocity (longitudinal component)
U	mean stream velocity
v	gas velocity (transverse component)
$\vec{w}$	=(u, v)
x	longitudinal coordinate
y	transverse coordinate
Y	mass fraction
W	molecular mass
$\vec{x}$	=(x, y)
.	scalar product
$\langle f(R)\rangle \circ g(\cdot)$	$=\int_0^\infty f(R)P(\vec{x},R)g(\cdot)dR$ or $\int_0^\infty \tilde{f}(R)\tilde{P}(\vec{x},r)g(\cdot)dr$ in dimensionless terms

Greek Symbols

∇	two dimensional gradient
ρ	density
α	the ratio of mass of liquid per unit volume to the gas density $\alpha = \frac{4}{3}\pi R_0^3 n_{d0}\rho_l / \rho_A$ (dimensionless)
σ	relate to a power law

Subscripts

0	initial
A	air
B	boiling
d	droplet
l	liquid
F	Fuel
o	oxygen
p	under constant pressure
s	spray

References

[1] Tambour Y., Vaporization of polydisperse fuel sprays in a laminar boundary layer flow: a sectional approach. Combustion and Flame, 58 (1984) 103-114.

[2] Tambour Y., A Lagrangian sectional approach for simulating droplet size distribution vaporizing fuel sprays in a turbulent jet. Combustion and Flame, 60 (1985) 15-28.

[3] Tambour Y., Zehavi S., Derivation of near-field sectional equations for the dynamics of polydisperse spray flows: An analysis of the relaxation zone behind a normal shock wave, Combustion and Flame, 95, (1993), 383-409.

[4] Katoshevski D., Tambour Y., A theoretical study of polydisperse liquid-sprays in a free shear-layer flow, Physics of Fluids A, 5, (1993) 3085-3098.

[5] Adeniji-Fashola A. and Chen C.P., Modeling of confined turbulent fluid-particle flows using Eulerian and Lagrangian schemes. International Journal of Heat and Mass Transfer, 33(4) (1990).

[6] A.A. Mostafa A.A., Mongia H.C., On the modeling of turbulent evaporating sprays: Eulerian versus Lagrangian approach. International Journal of Heat and Mass Transfer, 30(12) 1987.

[7] Elghobashi, S., Abou-Arab T., Rizk M., Mostafa A., Prediction of the particle-laden jet with a two-equation turbulence model. International Journal of Multiphase Flow, 10(6) (1984).

[8] F. A. Williams, Combustion theory, 2nd ed., Benjamin/Cummings, Menlo Park, CA, 1985.

[9] Archambault M.R., and Edwards C.F., Computation of Spray Dynamics by Direct Solution of Moment Transport Equations-Inclusion of Nonlinear Momentum Exchange, In 8th International Conference on Liquid Atomization and Spray Systems (ICLASS-2000), Pasadena.

[10] Beck J.C., Watkins A.P., On the Development of Spray Sub models Based on Droplet Size Moments. Journal of Computational Physics, 182(2) (2002).

[11] Beck J.C., Computational Modeling of Polydisperse Sprays without Segregation into Droplet Size Classes, Ph.D. thesis (UMIST, 2000).

[12] Beck J.C., and Watkins A.P., The droplet number moments approach to spray modeling: The development of heat and mass transfer sub-models, International Journal of Heat and Fluid Flow, 24(2) (2003).

[13] Watkins A.P., Three-dimensional modeling of gas flow and sprays in diesel engines, in Computer Simulation for Fluid-Flow. Heat and Mass Transfer and Combustion in Reciprocating Engines, edited by N. C. Markatos (Hemisphere, Washington, DC, 1989).

[14] Urzay J., Martinez-Ruiz D., Sánchez A.L., Li $\tilde{n}$ án A., Williams F.A., Flamelet structures in spray ignition. Center for Turbulence Research Annual Research Briefs 2013.

[15] Jafari H., and Seifi S., Solving a system of nonlinear fractional partial differential equations using homotopy analysis method. Communications in Nonlinear Science and Numerical Simulation, 14(5) (2009).

[16] Liao S.J., Beyond Perturbation: Introduction to the Homotopy Analysis Method. Boca Raton: CRC Press, Chapman & Hall, (2003).

[17] S.J. Liao, An optimal homotopy-analysis approach for strongly nonlinear differential equations, Communications in Nonlinear Science and Numerical Simulation 15 (2010) 2003-2016.